

Low-noise particle algorithms for extended magnetohydrodynamic closure^{a)}

D. C. Barnes,^{b)} J. Cheng, and S. E. Parker

Center for Integrated Plasma Studies, University of Colorado, Boulder, Colorado 80309, USA

(Received 15 November 2007; accepted 7 December 2007; published online 26 February 2008)

Two new low-noise particle closure methods are developed and tested. Closure of a small set of moment equations is accomplished with first or second order moments computed from a delta-f particle in cell (δf PIC) distribution. Conservation laws are developed and in one case apply to the discrete system, showing that squared weights are part of the system energy and therefore bounded for all time. Implicit time differencing and orbit averaging techniques are developed and implemented. Low-order moment constraints are satisfied exactly by a new particle representation. Numerical tests for one dimension, $k_{\perp}=0$, and two dimension, $k_{\parallel}=0$ show the successful application of both methods to damped waves and of the second order closure method to unstable gravitational modes. The methods described here are a natural and efficient way to close extended magnetohydrodynamic (MHD) equations to obtain a full kinetic description. © 2008 American Institute of Physics. [DOI: 10.1063/1.2839290]

I. INTRODUCTION

Simulation of magnetized plasmas in the case where collisions are infrequent presents a challenging computational problem. A variety of techniques, ranging from full fluid descriptions¹ to full particle simulation techniques² have been applied. All of these previous approaches compromise either fidelity to the physics which are to be represented or computational efficiency to achieve a low noise solution. That is to say, previous fluid approaches have included only a few of the many kinetic effects present in a low-collisionality plasma, while particle approaches have generally been restricted to smaller spatial and temporal scales and/or have often neglected magnetic perturbations.

In this paper, we explore the idea of combining fluid and particle equations to obtain algorithms which include all kinetic effects on low frequency plasma phenomena with sufficient efficiency that large scale, multidimensional computations can address realistic spatial and temporal scales. The general approach is to use a few of the low-order fluid equations and to compute the closure terms by low-noise particle approaches³ (δf methods). This type of approach has been previously described as hybrid, kinetic magnetohydrodynamic (MHD), or particle closure, but is more aptly named here the moment-particle (MP) approach. Given the current interest in the computational plasma community in combining and extending simulation codes, the developments presented here may be timely and useful.

An important feature of our work is the closure of the velocity moment hierarchy at low order. We have used either a particle derived current (current closure) or a particle derived stress (stress closure) to effect the closure. This feature stands in contrast to previously proposed approaches, such as, quiet implicit PIC (QIP) or Chapmann–Enskog-like (CEL),⁴ which require the calculation of third or fourth-order

velocity moments for closure of the moment equations. The present low-order approach offers two advantages over schemes requiring higher-order moments for closure: (1) the accurate and low-noise calculation of higher-order moments is more difficult because rare particles with high velocity make a greater contribution, in comparison with lower-order moments; (2) conservation laws provide an important connection between the moments and particles and only the first three such laws (particles, momentum, energy) have an obvious physical significance. Point (2) should become more obvious in the subsequent development here.

For low-frequency phenomena, an important algorithm issue is whether implicit time differencing can be applied. We show that stress closure admits implicit time differencing in a natural way, because of a nearly complete separation of the fluid and kinetic parts of the problem. In addition, particle substepping with orbit averaging⁵ can be incorporated and results in further improved computational efficiency. Implicit time differencing could also be combined with current closure, but this is not pursued here. Another essential (perhaps the most important) feature of the stress closure algorithm is that an energy conservation theorem exists for the discrete system. In addition to providing fidelity to the underlying physics and a sharp check on the numerics, the energy conservation shows that particle weights do not grow secularly in time, at least not indefinitely, resolving a problem which has been troublesome to δf methods in past applications.⁶ A similar result has been obtained recently in a more restrictive case.^{6,7}

We have tested both closure algorithms in simple cases where analytic solutions are known. For purposes of testing, electrons are treated as a massless fluid, and the ions as a collisionless kinetic species. Further, the polarization is restricted so that either k_{\perp} or k_{\parallel} vanishes. In the former case, tests of both current closure and stress closure are done in 1D, and two electromagnetic Alfvén modes and one electrostatic mode (ion-acoustic) are shown to be correctly recov-

^{a)}Paper BI2 1, Bull. Am. Phys. Soc. 52, 23 (2007).

^{b)}Invited speaker. Electronic mail: coronadocon@msn.com.

ered. In the latter case 2D stress closure calculations have addressed the gravitationally driven G-mode and shown agreement with previous theory while eliminating complicating physics associated with whistler and kinetic Alfvén wave physics.⁸ Extensions to full geometry are discussed but not fully developed in this paper.

During most of the past two decades, the present concepts have been discussed occasionally by the plasma simulation community.⁹ Progress toward practical implementations has been slow or nonexistent. Experience with QIP indicates that the success of any such algorithm is critically dependent on the implementation details. A comprehensive analytic theory which includes discretization issues is not yet available. (There is an extensive theory which can be applied in the limit of infinitely many simulation marker particles.¹⁰) Given the panoply of issues which arise from any particular implementation, it seems that the improvements introduced and described here have high value and are necessary for progress in implementation of such algorithms. In trite terms, the lamppost found here is a good place to search for MP algorithms.

The remainder of this paper is organized as follows: Section II derives the nonlinear implicit simulation equations. Section III discusses properties of the simulation models, while Sec. IV presents the results of numerical tests. Section V discusses extensions, while Sec. VI contains a summary and conclusions.

II. NONLINEAR TIME-IMPLICIT ALGORITHM

A. Moment equations

The evolution equations are equivalently the Vlasov equation (with the addition of both intra- and interspecies collision terms) or the infinite hierarchy of moment equations, combined with the appropriate Maxwell equations. For low-frequency applications considered here, the only Maxwell equations required are

$$\frac{\partial \mathbf{B}}{\partial t} = -\nabla \times \mathbf{E}, \quad \mathbf{J} = \frac{1}{\mu_0} \nabla \times \mathbf{B}, \quad (1)$$

where \mathbf{E} and \mathbf{B} are the electric field and the magnetic flux density, and where \mathbf{J} is the current density. System International (SI-MKS) units are used throughout.

Full electron physics are included by determining \mathbf{E} from the Ohm's law

$$\begin{aligned} en \left[\mathbf{E} - \eta \mathbf{J} + \left(\mathbf{u} - \frac{m}{M+m} \mathbf{u}_e \right) \times \mathbf{B} \right] \\ = \mathbf{J} \times \mathbf{B} - \nabla P_e - \nabla \cdot \mathbf{P}_e - \frac{\partial}{\partial t} m n \mathbf{u}_e, \end{aligned} \quad (2)$$

where P_e is the diagonal part of the electron stress tensor, and \mathbf{P}_e is the remainder, so that

$$P_e = \frac{\text{Tr}(\hat{\Pi}_e - m n \mathbf{u}_e \mathbf{u}_e)}{3}, \quad \mathbf{P}_e \equiv \hat{\Pi}_e - P_e \mathbf{1}, \quad (3)$$

$$\hat{\Pi}_e \equiv m \int \mathbf{v} \mathbf{v} \delta f_e d^3 v,$$

with M the ion mass, m the electron mass, and \mathbf{u} and \mathbf{u}_e the mass flow and electron fluid velocities. Notice that the electron Reynold's stress is included into \mathbf{P}_e (hence the "hat" on Π). The calculation of δf will be discussed subsequently.

As shown in Jones *et al.*,¹¹ Eq. (2) reduces to

$$\left[1 - \frac{c^2}{\omega_{pe}^2} \nabla^2 \right] \mathbf{E} = -\mathbf{u} \times \mathbf{B} + \eta \mathbf{J} + \mathbf{J} \times \mathbf{B} - \frac{1}{en} (\nabla P_e + \nabla \cdot \mathbf{P}_e), \quad (4)$$

in the appropriate limit of $m/M \ll 1$.

The inertia term of Eq. (4) can be important for microtearing, the generation of a parallel electric field and related inertial Alfvén wave physics. However, due to the small electron to ion mass ratio, this term is usually neglected for low-frequency meso-macro scale physics of the type being considered here. One essential effect of retaining this term is the resolution of the "low density" problem, in that the density occurs in the denominator of only one other term of Eq. (4). Thus, the finite electron mass model is simpler numerically than the zero electron mass model for systems with a near vacuum region.

The center of mass flow velocity \mathbf{u} in Eq. (4) is to a very good approximation

$$\mathbf{u} = \mathbf{u}_i + \frac{m}{M} \mathbf{u}_e. \quad (5)$$

Equations (1)–(5) may be closed without introducing additional moment equations. The species velocities \mathbf{u}_α where $\alpha=(e,i)$ may be determined from the particle distribution function

$$\mathbf{u}_\alpha = \frac{1}{n} \int \mathbf{v} \delta f_\alpha d^3 v. \quad (6)$$

Due to quasineutrality $n_i = n_e \equiv n$,

$$n = \bar{n} + \int \delta f d^3 v, \quad (7)$$

where we have introduced the convention of denoting equilibrium or background quantities by an overbar here and in the sequel.

As a first approximation, it will be assumed that $n \approx \bar{n}$ in the denominators of Eqs. (4) and (6). Dropping the electron inertia term was already briefly discussed, and there are other interesting limits of this model. If the electron pressure term is neglected in the generalized Ohm's law (a typical limit in resistive MHD), and $m/M \rightarrow 0$ in Eq. (2), which is a reasonable assumption assuming $\mathbf{u}_e \ll v_{te}$, one obtains the interesting limit where the system is completely closed by keeping ion kinetics only. This is consistent with assuming the MHD momentum equation describes primarily ion flow dynamics.

Similar models have been used in the past. The models were used to study kinetic effects on problems generally studied using MHD. In 1999, a model that used full particle in cell (PIC), instead of δf , to solve for the kinetics was used to study collisionless magnetic reconnection.^{12–18} In 2000, Belova used another model that incorporated the δf method, but neglected the electron inertia term, to study the tilt instability in field-reversed configurations.^{19–22} The current closure model proceeds as described to this point, with the evolution of δf given in the next section.

An alternative approach to the current closure scheme is to introduce one additional moment equation, the total momentum equation

$$Mn \frac{D\mathbf{u}}{Dt} = Mng + \mathbf{J} \times \mathbf{B} - \nabla P_e - \nabla \cdot \mathbf{P}_e - \nabla \cdot \Pi_i, \quad (8)$$

where gravity \mathbf{g} has been included for subsequent applications. Some terms of order m/M have again been neglected in Eq. (8). The notation for the time derivative is standard, with D/Dt representing the convective ion frame derivative

$$\frac{D}{Dt} = \frac{\partial}{\partial t} + \mathbf{u} \cdot \frac{\partial}{\partial \mathbf{x}}. \quad (9)$$

(We will use interchangeably the notations ∇ and $\partial/\partial \mathbf{x}$, with the latter useful to distinguish the spatial derivative from the velocity derivative in kinetic equations.) The stress closure model uses the equations to this point, with the ion stress determined from the δf as described in the next section.

In many applications, simplified electron physics can be used. In the sequel, we will simplify the electron physics by neglecting the electron inertia term of Eq. (4), as already discussed and include only the scalar electron pressure. These neglected terms are not important for our present purposes and are easily reinserted into the model when required. To close the model without kinetic electron effects, we add the evolution equations for density and electron pressure

$$\frac{Dn}{Dt} + n \nabla \cdot \mathbf{u} = 0, \quad (10)$$

$$\frac{\partial P_e}{\partial t} + \mathbf{u}_e \cdot \nabla P_e + \Gamma_e P_e \nabla \cdot \mathbf{u}_e = 0,$$

where the electron velocity is given from the definition of the current density as

$$\mathbf{u}_e = \mathbf{u} - \frac{\mathbf{J}}{en}. \quad (11)$$

The first equation of Eq. (10) is an alternative way to evolve the density, compared with the kinetic calculation of Eq. (7). The distinction between these two approaches is developed further in the sequel.

It remains to specify the ion velocity (for current closure) or ion pressure tensor Π_i (for stress closure). The ion stress is determined by the solution of the ion Vlasov equation which we take up next.

B. δf equations

Ions are described by the Vlasov equation

$$\frac{\delta f}{\delta t} + \mathbf{v} \cdot \frac{\partial f}{\partial \mathbf{x}} + \frac{e}{M} (\mathbf{F} + \mathbf{v} \times \mathbf{B}) \cdot \frac{\partial f}{\partial \mathbf{v}} = 0, \quad (12)$$

where \mathbf{v} is the single particle velocity, and where the effective electric field \mathbf{F} contains the gravity also.

Equation (12) is solved by finding a correction to a background distribution using the PIC method. We have used two different δf schemes for the two different closures schemes. On the one hand, the current closure uses a conventional, fixed-background approach. On the other hand, the stress closure uses an evolving background approach. To minimize confusion, we will use the notation δf to refer to the correction relative to a fixed background and the notation \bar{f} to refer to the different correction relative to an evolving background.

1. Current closure

Here, we describe how δf is evolved to evaluate the fluid moments in the generalized Ohm's law, Eq. (4). Vlasov's equation (12) is used. Gyrokinetic or drift-kinetic equations could also be used if these are appropriate limits for a given problem.³

It is assumed that an equilibrium distribution function \bar{f} exists, and only the perturbed part of the distribution function is evolved

$$\begin{aligned} \frac{d\delta f_\alpha}{dt} &\equiv \frac{\partial \delta f_\alpha}{\partial t} + \mathbf{v} \cdot \frac{\partial \delta f_\alpha}{\partial \mathbf{x}} + \frac{q_\alpha}{m_\alpha} (\mathbf{F} + \mathbf{v} \times \mathbf{B}) \cdot \frac{\partial \delta f_\alpha}{\partial \mathbf{v}} \\ &= - \frac{q_\alpha}{m_\alpha} (\mathbf{F} + \mathbf{v} \times \mathbf{B}) \cdot \frac{\partial \bar{f}_\alpha}{\partial \mathbf{v}}, \end{aligned} \quad (13)$$

where $f = \bar{f} + \delta f$. The equilibrium \bar{f} is taken to be a Maxwellian distribution in the numerical tests presented here, which is typical. The term $\partial \bar{f}_\alpha / \partial t + \mathbf{v} \cdot \nabla \bar{f}_\alpha$ is not included since this is the total time derivative of \bar{f} , which is taken to be zero since \bar{f} is the equilibrium state. It is straightforward to implement any equilibrium \bar{f} , but choosing a particular case will make the presentation of the model clearer. For a Maxwellian equilibrium distribution function the velocity derivative is given by

$$\frac{\partial \bar{f}}{\partial \mathbf{v}} = \frac{\partial f_M}{\partial \mathbf{v}} = - \frac{\mathbf{v}}{\bar{v}_i^2} f_M, \quad (14)$$

where $\bar{v}_i = \sqrt{k_B T / m}$. Hence, Eq. (13) can be written in characteristic form

$$\frac{d}{dt} \delta f_\alpha = \frac{q_\alpha}{m_\alpha \bar{v}_{i,\alpha}^2} \mathbf{v} \cdot \mathbf{E} f_M. \quad (15)$$

The $\mathbf{v} \times \mathbf{B}$ term does not contribute to the evolution equation for δf for an expansion about Maxwellian equilibrium distribution. This equation can be solved using the δf method where δf is represented in the following way:

$$\delta f(\mathbf{z}, t) = \sum_i \delta f_i \Delta V_i \delta(\mathbf{x} - \mathbf{x}_i) \delta(\mathbf{v} - \mathbf{v}_i), \quad (16)$$

where ΔV_i is the amount of phase space volume associated with the i th marker particle,²³ and the PIC method (with linear interpolation) is used to evaluate grid depositions. In this paper a uniform phase space loading (particles are started with a uniform distribution in velocity and real space) is used, so that $\Delta V_i = \text{const.}$ is the same for every particle. Other loadings (e.g., velocity-weighted Maxwellian) have also been tried with similar or inferior results. The species subscript is omitted from Eq. (16) and in the sequel, without loss of generality. In our tests to date, only the ion distribution is evolved, so one may assume that we are discussing the ion distribution function from this point forward.

2. Stress closure

One could develop a stress closure scheme which parallels the previous current closure scheme. It develops, however, that this approach is not accurate or useful. There seems only one way in which a stress closure scheme can be made to work with an achievable number of particles, and we develop this scheme here. We adopt an evolving background approach, in which the previously described QIP method is modified by using a fixed temperature background distribution, rather than one with an evolving temperature. In this paper, we will consider the simplest case of uniform background temperature, as this is sufficient for our present testing, and extension to full temperature gradient introduces complications which will be dealt with in subsequent work. The algorithm for the case of temperature gradient is outlined in Sec. VI where extensions to the present restricted scope are discussed.

The unknown distribution is again separated into a background and a correction part. The background evolves according to the solution of the moment equations. Thus,

$$f = \bar{f} + \tilde{f}, \quad \bar{f} = \frac{n}{(\sqrt{2\pi}\bar{v}_T)^3} e^{-w^2/2\bar{v}_T^2}, \quad (17)$$

where the particular velocity $\mathbf{w} = \mathbf{v} - \mathbf{u}$, with n and \mathbf{u} determined from the solution of the moment equations of the previous subsection. Here and in the sequel perturbation or fluctuating quantities are denoted by a tilde.

The analog of Eq. (13) is

$$\frac{d\tilde{f}}{dt} = -\frac{\partial \tilde{f}}{\partial t} - \mathbf{v} \cdot \frac{\partial \tilde{f}}{\partial \mathbf{x}} - \frac{d\mathbf{w}}{dt} \cdot \frac{\partial \tilde{f}}{\partial \mathbf{w}}, \quad (18)$$

where the individual ion orbits are given by

$$\dot{\mathbf{x}} = \mathbf{v}, \quad \dot{\mathbf{v}} = \frac{e}{M} (\mathbf{F} + \mathbf{v} \times \mathbf{B}). \quad (19)$$

An essential feature of our stress closure algorithm is the use of \mathbf{w} in place of \mathbf{v} . Using Eqs. (8) and (19) we find the evolution equation for the particular velocity to be independent of the electric field

$$\dot{\mathbf{x}} = \mathbf{w} + \mathbf{u}, \quad (20)$$

$$\dot{\mathbf{w}} = \frac{e}{M} \mathbf{w} \times \mathbf{B} - \mathbf{w} \cdot \frac{\partial \mathbf{u}}{\partial \mathbf{x}} + \bar{v}_T^2 \frac{1}{n} \frac{\partial n}{\partial \mathbf{x}} - \tilde{\mathbf{A}},$$

where the ion stress acceleration has been separated into two parts due to \bar{f} and \tilde{f} , respectively,

$$-\frac{\nabla \cdot \Pi_i}{Mn} = -\frac{k_B \bar{T} \nabla n}{Mn} + \tilde{\mathbf{A}}, \quad (21)$$

$$\tilde{\mathbf{A}} = -\frac{1}{n} \nabla \cdot \int d\mathbf{w} \tilde{f} \mathbf{w} \mathbf{w}.$$

In the sequel, it is more convenient to replace \tilde{f} with the perturbation weights $\tilde{h} = \tilde{f}/(\bar{f} + \tilde{f})$, which satisfy

$$\frac{\dot{\tilde{h}}}{1 - \tilde{h}} = -\frac{\partial \log \bar{f}}{\partial t} - \mathbf{v} \cdot \frac{\partial \log \bar{f}}{\partial \mathbf{x}} - \frac{d\mathbf{w}}{dt} \cdot \frac{\partial \log \bar{f}}{\partial \mathbf{w}}. \quad (22)$$

Direct substitution of Eqs. (10) and (20) gives the evolution equation

$$\frac{\dot{\tilde{h}}}{1 - \tilde{h}} = \nabla \cdot \mathbf{u} - \frac{1}{\bar{v}_T^2} \left(\mathbf{w} \mathbf{w} : \frac{\partial \mathbf{u}}{\partial \mathbf{x}} + \mathbf{w} \cdot \tilde{\mathbf{A}} \right), \quad (23)$$

leading, as previously, to

$$\tilde{f}(\mathbf{z}, t) = \sum_i W_i \tilde{h}_i \delta(\mathbf{x} - \mathbf{x}_i) \delta(\mathbf{w} - \mathbf{w}_i). \quad (24)$$

Since \tilde{h} is the ratio of the correction to the full distribution, the initial marker particle distribution is characterized by the *a priori* weights $\{W_i\}$, which now include the phase space volume element and the initial Maxwellian distribution.

The usual PIC (Klimentovich) representation of Eq. (24) is not the most useful to us, since \tilde{h} is constrained so that its first two \mathbf{w} moments vanish. Accordingly, we replace the velocity space delta function by its projection with these moments removed. Formally, one can expand δ as a series of Hermite polynomials and then remove the terms which contribute to the low-order moments. The replacement required is thus found to be

$$\delta \rightarrow \delta(\mathbf{w} - \mathbf{w}_i) - \bar{f}(\mathbf{w}_i) \left(1 + \frac{\mathbf{w} \cdot \mathbf{w}_i}{\bar{v}_T^2} \right). \quad (25)$$

Next, we integrate the particle shape (now in both \mathbf{x} and \mathbf{w}) against the driving terms and the phase space integrals required. The resulting final stress closure PIC equations are

$$\frac{\dot{\tilde{h}}_i}{1 - \tilde{h}_i} = \sum_g s(\mathbf{x}_g - \mathbf{x}_i) \left(\frac{\partial}{\partial \mathbf{x}_g} \cdot \mathbf{u} - \frac{\mathbf{w}_i \mathbf{w}_i}{\bar{v}_T^2} : \frac{\partial \mathbf{u}}{\partial \mathbf{x}_g} \right) \quad (26)$$

$$\tilde{\mathbf{A}}_g = -\sum_i W_i \tilde{h}_i (\mathbf{w}_i \mathbf{w}_i - \bar{v}_T^2 \mathbf{1}) \cdot \frac{\partial}{\partial \mathbf{x}_g} s(\mathbf{x}_g - \mathbf{x}_i) \Big/ n \Delta_g,$$

plus the modified orbit Eqs. (20). In Eq. (26), s is the particle shape (interpolation function), the subscript g indicates grid

points, and Δ_g is the cell volume in configuration space, which is assumed to be constant here.

Notice that two previously identified troublesome features of evolving background δf methods have been solved by the projection of Eq. (26). First, the contribution to the closure stress reflects the constraints which \tilde{f} must satisfy. Second, the implicit occurrence of the closure moment in the evolution equation for \tilde{f} [Eq. (23)] is eliminated by the projection. Notice also that there exists a symmetry between the kernel of the \tilde{h}_i evolution equation and the closure moment. This will lead to favorable conservation properties, which we discuss in the sequel.

III. PROPERTIES OF THE DISCRETE SYSTEMS

In this section, several numerical issues are discussed. The particle time stepping issues are discussed next, followed by the moment time stepping issues. The following subsection discusses the conservation properties of the two schemes, while the remaining subsections discuss issues related to spatial centering and obtaining derivatives of moment quantities for the particle step of the stress closure scheme.

A. Particle equations time step

In comparison with other PIC implementations, both of our closure schemes require the time advancement of equations of the form $\dot{x}=f(x)$ for which the usual leapfrog is not applicable. We have employed modified leapfrog schemes, either using a single time level or two time levels to resolve this difficulty. For example, the two-level scheme for advancing the current closure particle equations are

$$\begin{aligned} \mathbf{x}^* &= \mathbf{x}^{n-1} + 2\Delta t \mathbf{v}^n, \\ \mathbf{v}^* &= \mathbf{v}^{n-1} + 2\Delta t \frac{q_\alpha}{m_\alpha} (\mathbf{E}^n + \mathbf{v}^n \times \mathbf{B}^n), \end{aligned} \quad (27)$$

$$\delta f_\alpha^* = \delta f_\alpha^{n-1} + 2\Delta t \frac{q_\alpha}{m_\alpha v_{T,\alpha}^2} \mathbf{v}^n \cdot \mathbf{E}^n f_M^n,$$

where the superscript * denotes a predicted $n+1$ time level, followed by the corrector advance,

$$\begin{aligned} \mathbf{x}^{n+1} &= \mathbf{x}^n + \frac{\Delta t}{2} (\mathbf{v}^n + \mathbf{v}^*), \\ \mathbf{v}^{n+1} &= \mathbf{v}^n + \frac{\Delta t}{2} \frac{q_\alpha}{m_\alpha} (\mathbf{E}^n + \mathbf{v}^n \times \mathbf{B}^n + \mathbf{E}^* + \mathbf{v}^* \times \mathbf{B}^*), \\ \delta f_\alpha^{n+1} &= \delta f_\alpha^n + \frac{\Delta t}{2} \frac{q_\alpha}{m_\alpha v_{T,\alpha}^2} (\mathbf{v}^n \cdot \mathbf{E}^n + \mathbf{v}^* \cdot \mathbf{E}^*) f_M^n, \end{aligned} \quad (28)$$

where the predicted fields are obtained in exactly the same manner as the predictor advance of Eq. (27), and the corrected fields are obtained in the same manner as the corrector advance of Eq. (28).

An alternative approach is to use a single time level modified leapfrog in which the same predictor-corrector

strategy is used to obtain time centering. Thus, the nonlinear orbit Eqs. (20) are advanced to obtain a predictor as

$$\mathbf{x}^* = \mathbf{x}^{n-1/2} + \Delta t [\mathbf{w}^n + \mathbf{u}^n(\mathbf{x}^{n-1/2})], \quad (29)$$

$$\begin{aligned} \mathbf{w}^* &= \mathbf{w}^n + \Delta t \left[\frac{e}{M} \frac{\mathbf{w}^* + \mathbf{w}^n}{2} \times \mathbf{B}^{n+1/2} - \mathbf{w}^n \right. \\ &\quad \left. \cdot \frac{\partial \mathbf{u}^{n+1/2}}{\partial \mathbf{x}} + \frac{\bar{v}_T^2}{n} \frac{\partial n^{n+1/2}}{\partial \mathbf{x}} - \tilde{\mathbf{A}}^{n+1/2} \right] (\mathbf{x}^*), \end{aligned}$$

and then to get the final corrector time advance as

$$\mathbf{x}^{n+1/2} = \mathbf{x}^{n-1/2} + \Delta t \left[\mathbf{w}^n + \mathbf{u}^n \left(\frac{\mathbf{x}^{n-1/2} + \mathbf{x}^*}{2} \right) \right], \quad (30)$$

$$\begin{aligned} \mathbf{w}^{n+1} &= \mathbf{w}^n + \Delta t \left[\frac{e}{M} \frac{\mathbf{w}^{n+1} + \mathbf{w}^n}{2} \times \mathbf{B}^{n+1/2} - \frac{\mathbf{w}^* + \mathbf{w}^n}{2} \cdot \frac{\partial \mathbf{u}^{n+1/2}}{\partial \mathbf{x}} \right. \\ &\quad \left. + \frac{\bar{v}_T^2}{n} \frac{\partial n^{n+1/2}}{\partial \mathbf{x}} - \tilde{\mathbf{A}}^{n+1/2} \right] (\mathbf{x}^{n+1/2}). \end{aligned}$$

The velocity advance equations of Eqs. (29) and (30) are of a form to which the method of Boris²⁴ is applied.

Notice that both these modified leapfrog steps preserve the perpendicular gyration velocity, the first by three level time centering and the second by a Boris-type velocity advance.

B. Moment equations time step

Since the current closure particle advance requires both the \mathbf{E} and \mathbf{B} fields at the same time level, the three level scheme of Eqs. (27) and (28) is used to advance the field quantities also. Only \mathbf{B} is time advanced, as the remaining field equations contain no time derivatives.

The stress closure moment equations are exactly those of two-fluid extended MHD, with the ion adiabatic index of unity. We solve these implicitly using Sovinec's time-centered implicit leapfrog.¹ The same separation into background or equilibrium and perturbation quantities used in Ref. 1 is employed here. The only extension is associated with the electron inertia and tensor electron stress terms of Eq. (4). Since these do not involve additional time derivatives, there is no modification to the time step scheme of Ref. 1. The particle closure introduces an additional term into the momentum equation. This is made time centered by iterating the particle advance, which depends on the velocity \mathbf{u} and using the time average of \mathbf{u} in this particle advance. The main advantage of this approach is that orbit averaging can be easily included, and this is used for the G-mode tests of the sequel. Figure 1 shows the coupling scheme schematically. The overall scheme is unconditionally stable and Δt can be chosen to resolve the mode of interest. The smaller δt which is used to substep the particles is chosen to resolve the orbital frequencies of individual marker particles.

C. Conservation laws

It has been shown that the current closure equations conserve energy in the limit of many particles and small time

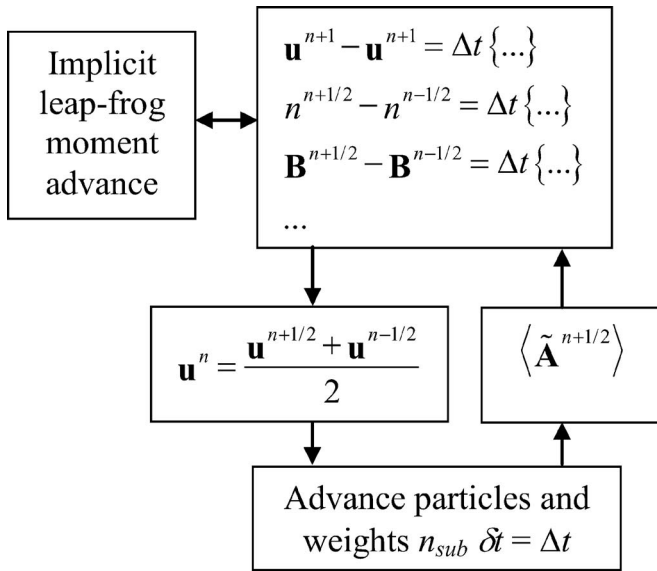


FIG. 1. Implicit time scheme for stress closure. Loop indicated by arrows is iterated until change in closure becomes small.

step.¹⁰ The stress closure scheme admits an energy conservation law which applies for a finite particle number and arbitrary Δt . This follows from Eq. (26). Taking the dot product of the $\tilde{\mathbf{A}}$ equation with $n\mathbf{u}$ and integrating (summing) over the grid points and comparing the result with multiplying the \tilde{h} equation with \tilde{h} and summing over all particles gives the identity

$$\frac{d}{dt} \left\{ -M\bar{v}_T^2 \sum_i W_i [\log(1 - \tilde{h}_i) + \tilde{h}_i] \right\} = -M \sum_g \Delta_g n_g \mathbf{u}_g \cdot \tilde{\mathbf{A}}_g. \quad (31)$$

The remainder of the energy conservation law is developed in the Appendix, and shows that the quantity in brackets on the left-hand side of Eq. (31) is part of the conserved total energy of the system. As the remaining terms are positive definite, the bracketed quantity is bounded for all time. Further, for small weights, to a very good approximation

$$-\sum_i W_i [\log(1 - \tilde{h}_i) + \tilde{h}_i] \approx \frac{1}{2} \sum_i W_i \tilde{h}_i^2, \quad (32)$$

so that a part of the system energy is proportional to the rms particle weight. In this way, the particle weights are absolutely bounded for all time. A similar result in a more restrictive setting was given recently by Dimits.⁷ When orbit averaging is used, it is easy to arrange time centering so that the difference of the particle weight sum telescopes over substeps. Thus, writing fore-superscripts to indicate particle (δt) time levels

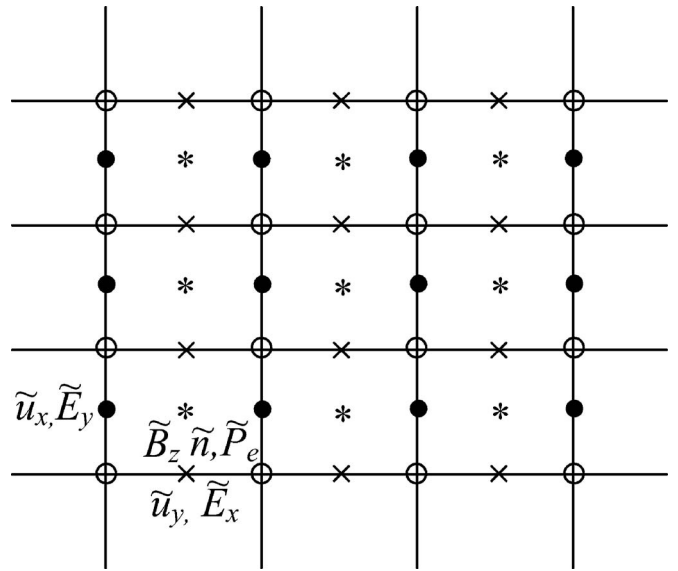


FIG. 2. Centering of components uses various interleaved meshes.

$$\begin{aligned} \frac{1}{2} \sum_i W_i ({}^{p+1}\tilde{h}_i^2 - {}^p\tilde{h}_i^2) &= \sum_i W_i \frac{{}^{p+1}\tilde{h}_i + {}^p\tilde{h}_i}{2} ({}^{p+1}\tilde{h}_i - {}^p\tilde{h}_i) \\ &\Rightarrow \frac{1}{2} \sum_i W_i ({}^{p+n_{sub}}\tilde{h}_i^2 - {}^p\tilde{h}_i^2) \\ &= \sum_{s=0}^{n_{sub}-1} \sum_i W_i ({}^{p+s+n_{sub}}\tilde{h}_i^2 - {}^{p+s}\tilde{h}_i^2). \end{aligned} \quad (33)$$

It follows that the identity of Eq. (31) is exact, if the closure moment is computed using the average of the weights $({}^{p+1}\tilde{h}_i + {}^p\tilde{h}_i)/2$ over the particle steps.

Having a conserved energy which contains the rms particle weights leads to improved numerical properties. The rms weight is bounded for all time, as previously noted. Further, it seems likely that there exists a fluctuation-dissipation theorem for the discrete system, based on the discrete conserved energy. The consideration of this and related statistical mechanics issues are beyond our present scope, but may form the basis for interesting future work.

D. Spatial centering issues

To maintain energy conservation and $\nabla \cdot \mathbf{B} = 0$ in the spatially discrete system, several approaches are possible. For example, one can locate all moment quantities on the same (usually uniform) mesh and add a diffusive term $\kappa_d \nabla(\nabla \cdot \mathbf{B})$ to the right-hand side of Eq. (1) to maintain $\nabla \cdot \mathbf{B} = 0$. Alternatively, a Yee mesh²⁵ may be used to assure conservation properties.

In our 2D tests with stress closure, a Yee mesh has been used. The centering of various quantities is shown in Fig. 2.

The interleaved meshes assure that $\nabla \cdot \mathbf{B} = 0$, even for extensions to the full geometry (see Sec. VI). Energy conservation requires that the finite difference forms of

$$\mathbf{u} \cdot \mathbf{J} \times \mathbf{B} + \mathbf{J} \cdot \mathbf{u} \times \mathbf{B} = 0, \quad \mathbf{J} \cdot \mathbf{J} \times \mathbf{B} = 0, \quad (34)$$

are satisfied. The remaining vector calculus identities are automatically satisfied by using centered differences on the Yee mesh. The first of these algebraic identities is facilitated by using the Maxwell stress form for $\mathbf{J} \times \mathbf{B}$ and averaging \mathbf{B} from cell centers to edges to evaluate $\mathbf{u} \times \mathbf{B}$ on the same mesh. The second is satisfied by defining $\mathbf{J} \times \mathbf{B}$ with a four-point average from the four neighboring edges to a given edge.

E. Gradient of moment quantities

One additional issue for the stress closure approach is dealing with the gather and scatter quantities in a symmetric way and avoiding computing numerical derivatives. For this, the terms of Eq. (26) which contain a spatial derivative are approximated by two interpolations as follows:

$$\begin{aligned} \delta t \mathbf{w}_i \mathbf{w}_i: \frac{\partial \mathbf{u}}{\partial \mathbf{x}} &\approx \mathbf{w}_i \cdot [\mathbf{u}(\mathbf{x}_i + \delta t \mathbf{w}_i/2) - \mathbf{u}(\mathbf{x}_i - \delta t \mathbf{w}_i/2)] \\ &\approx \mathbf{w}_i \cdot \sum_g [s(\mathbf{x}_g - \mathbf{x}_i + \delta t \mathbf{w}_i/2) \\ &\quad - s(\mathbf{x}_g - \mathbf{x}_i - \delta t \mathbf{w}_i/2)] \mathbf{u}_g. \end{aligned} \quad (35)$$

Symmetry required for energy conservation is maintained by using the same rule for the scatter of the ion stress to the mesh

$$\begin{aligned} \delta t \frac{\partial}{\partial \mathbf{x}_g} \cdot \sum_i \tilde{h}_i \mathbf{w}_i \mathbf{w}_i s(\mathbf{x}_g - \mathbf{x}_i) &\approx \sum_i \tilde{h}_i \mathbf{w}_i \delta t \mathbf{w}_i \cdot \frac{\partial}{\partial \mathbf{x}_g} s(\mathbf{x}_g - \mathbf{x}_i) \\ &\approx \sum_i \tilde{h}_i \mathbf{w}_i [s(\mathbf{x}_g - \mathbf{x}_i + \delta t \mathbf{w}_i/2) \\ &\quad - s(\mathbf{x}_g - \mathbf{x}_i - \delta t \mathbf{w}_i/2)]. \end{aligned} \quad (36)$$

It is clear that multiplying Eq. (36) by $\mathbf{u}_g \cdot$ and summing over the mesh gives the negative of the result of multiplying Eq. (37) by \tilde{h}_i and summing over the particles, which is the required condition for the energy conservation theorem of the Appendix.

IV. NUMERICAL TESTS

We have implemented the closure schemes developed previously in 1D and 2D codes. The time step is exactly as described, except that only linear tests have been done, for the most part. In addition, because it is usually not required, orbit averaging has not been implemented in the 1D versions. The current closure scheme has been implemented in a 1D code, while the stress closure scheme has been implemented in both a 1D (IMP1 for implicit moment-particle 1D) and a 2D version (IMP2).

One-dimensional tests were carried out for a uniform plasma and for $k_\perp=0$. The evolved particle quantities are $\delta f, z, v_x, v_y, v_z$ and the perturbed field quantities are $E_x(z), E_y(z), E_z(z), B_x(z), B_y(z)$.

For cold ions, assuming $\mathbf{u}=\mathbf{u}_i$ and $\Pi_e=0$. The dispersion relation is the following:

$$\begin{aligned} &\left[1 + \left(\frac{ck}{\omega_{pe}} \right)^2 + \frac{\Omega_i^2}{(\omega^2 - \Omega_i^2)} + i \frac{k^2 \eta}{\mu_0 \omega} \right]^2 \\ &= \left[\frac{k^2 v_A^2}{\omega \Omega_i} + \frac{\omega \Omega_i}{(\omega^2 - \Omega_i^2)} \right]^2. \end{aligned} \quad (37)$$

Taking the zero resistivity limit ($\eta=0$), Eq. (37) can be solved exactly and has four roots, two pairs that are identical except for having an opposite sign. The roots are

$$\begin{aligned} \omega = &\frac{\pm \Omega_i}{2 \left[1 + \left(\frac{ck}{\omega_{pe}} \right)^2 \right]} \left\{ \left(\frac{kv_A}{\Omega_i} \right)^2 - \left(\frac{ck}{\omega_{pe}} \right)^2 \right. \\ &\left. \pm \sqrt{\left[\left(\frac{kv_A}{\Omega_i} \right)^2 + \left(\frac{ck}{\omega_{pe}} \right)^2 \right]^2 + 4 \left(\frac{kv_A}{\Omega_i} \right)^2} \right\}. \end{aligned} \quad (38)$$

There are two interesting limits corresponding to the whistler wave and the Alfvén wave. First, the whistler wave dispersion relation with inertial corrections is obtained by assuming $k^2 v_A^2 / \Omega_i^2 \gg 1$ and $c^2 k^2 / \omega_{pe}^2 \ll k^2 v_A^2 / \Omega_i^2$. Second, the Alfvén wave is obtained by assuming $k^2 v_A^2 / \Omega_i^2 \ll 1$ along with $c^2 k^2 / \omega_{pe}^2 \ll k^2 v_A^2 / \Omega_i^2$. Equation (38) then reduces to

$$\omega^2 = \frac{k^2 v_A^2}{\left(1 + \frac{c^2 k^2}{\omega_{pe}^2} \right)^2}, \quad (39)$$

which is the inertial Alfvén wave dispersion relation. The finite Larmor radius corrections to Eq. (39), which depend on $k_\perp \neq 0$ are included in the current closure simulation model through δf .

Figure 3 shows a comparison of the simulation to the dispersion relation given in Eq. (38), showing good agreement and demonstrating the method. Also shown, is the ion acoustic wave branch. All three modes are simultaneously present in the simulation and frequency spectra is used to generate the mode frequencies. All the simulations presented used 2000 ion particles. No kinetic electron effects are retained and no electron inertia effects are kept so that $m_e=0$ and $c/\omega_{pe}=0$. The time step was $\Delta t=0.01/\Omega_{ci}$. For Fig. 3, $v_{Ti}=0.15V_A$ and $T_e/T_i=16$. The wave number kd_i ranges 0.5–2, where d_i is the collisionless ion skin depth.

To model ion acoustic waves we use the electron pressure Eq. (10) with $\Gamma_e=1$ [a simple isothermal electron approximation for the electron pressure. $(-1/en_0 \nabla \cdot \Pi_e)$ term to Ohm's law]. This term is simple to evaluate assuming the adiabatic electron response, and quasineutrality

$$\nabla \cdot \Pi_e = T_e \nabla n_e = T_e \nabla n_i. \quad (40)$$

Since the ion density only varies in the \hat{z} direction, inclusion of this term will only effect E_z , and the two transverse waves will be unchanged. Inclusion of this term has the affect of adding the longitudinal electrostatic ion acoustic wave. Figure 4 shows a comparison of the numerical (real frequency shown by “×,” damping by “◇”) and analytic ion kinetic dispersion relation (solid curves) indicating good agreement with linear theory for the ion acoustic wave. The parameters for the simulations shown in Fig. 4 were the same as above

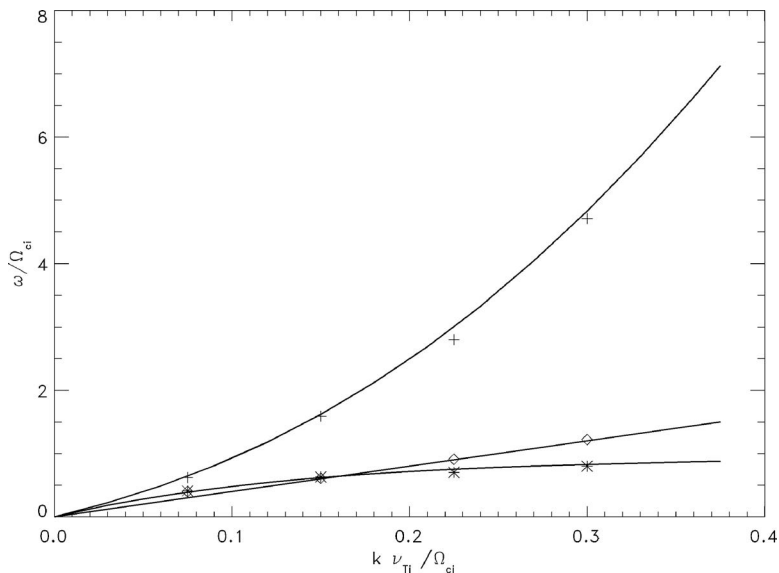


FIG. 3. Three wave frequencies vs k_{\parallel} .

in Fig. 2 except now $kd_i=2$, $T_e/T_i=4$, and v_{Ti}/V_A ranges 0.25–1.

The ion-acoustic wave has also been tested with IMP1. Results for the real frequency (“*”) and damping (“Δ”) of the wave are shown in Fig. 4 and compared with the results from the current closure scheme and the analytic solution. As can be seen, good agreement is obtained with both methods.

The stress closure algorithm described in the previous sections has also been implemented in the two-dimensional code IMP2. The present implementation is restricted to TE polarization (\mathbf{E} in simulation plane, \mathbf{B} normal), and is linearized. The G-mode has been observed in a case with density gradient described by an exponential profile $\bar{n}=n_0e^{x/L}$. The equilibrium temperature is uniform, the equilibrium magnetic field is determined from pressure balance to support the resulting pressure gradient and the gravity, which is assumed uniform in the $-x$ direction. The dispersion relation for this case has been obtained including both the Rayleigh–Taylor²⁶ and the Parker drives.²⁷ The resulting growth rate is

$$\gamma_M^2 = \frac{g}{L} + \frac{g^2}{C^2}, \tag{41}$$

where g is the gravity and C is the magnetoacoustic speed.

We have carried out two series of calculations in which parameters were adjusted so that $k\rho_i$ is of order unity. In each series, the value of $k\rho_i$ was varied by varying k (where k is the wavenumber in the y direction normal to the density gradient) while all other parameters were held fixed. In the first, low β series, the parameters were

$$\beta = 0.02, \quad T_e/T_i = 0, \quad X/L = 0.00833, \quad L/d_i = 5270.0,$$

$$g/d_i\Omega_{ci}^2 = 5.317 \times 10^{-4}; \quad \gamma_M/\Omega_{ci} = 6.168 \times 10^{-4},$$

where X is the domain size in the x direction of the density gradient, and d_i is based on n_0 . The MHD growth rate is dominated by the Parker term. The gyroradius parameter $k\rho_i$ varied from 0.001450 to 0.2861.

Results were obtained for these parameters by an initial

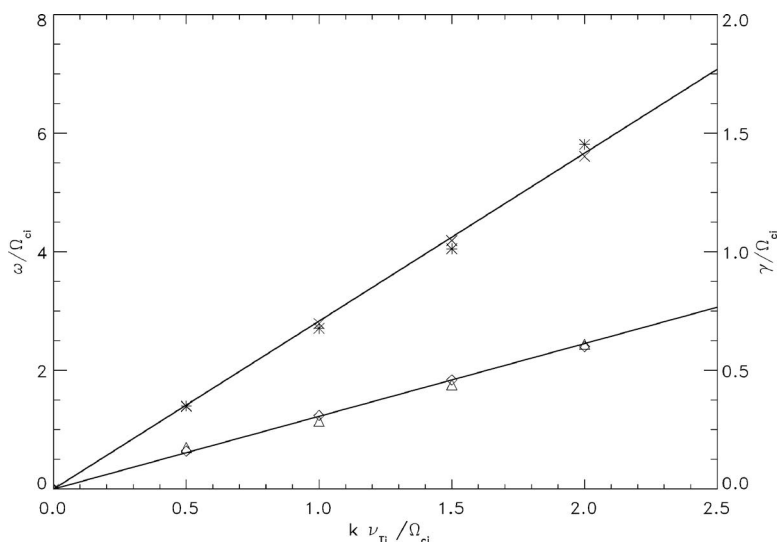


FIG. 4. Ion-acoustic real frequency (upper plot) and damping (lower plot) vs k_{\parallel} .

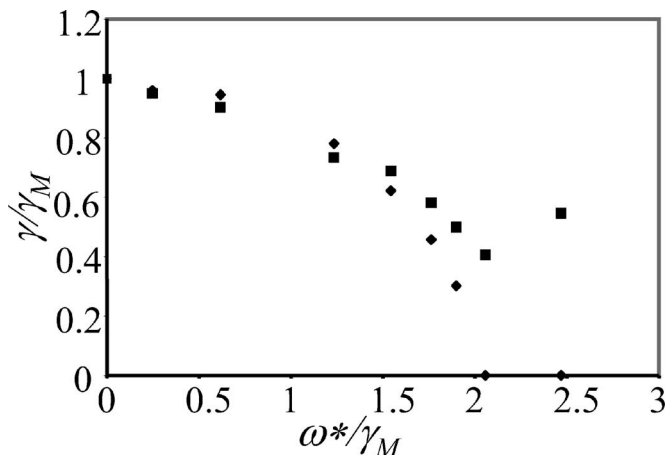


FIG. 5. Variation of growth rate with k for the low β case.

value calculation using IMP2. The mesh used was 30×16 , $\delta t = \Delta t / 80 = 0.4311 / \Omega_{ci}$, and 9 particles per cell were loaded with various high v weighted distributions. For example, markers were loaded uniformly in velocity between $\pm 5 v_T$, or with some superposition of the background Maxwellian weighted by a combination of v^2 and v^4 terms. Smoother results and more rapid convergence were observed with the velocity weighted Maxwellian, so this distribution was used for most of the results described here.

Growth rates are shown in Fig. 5, where both the growth rate and the drift frequency are scaled with γ_M . Results of two distinct calculations are shown. The diamonds indicate results in which all moment equations were time advanced, but the ion stress closure was not included, while the squares show the results with full stress closure.

The MHD growth rate calculated from Eq. (41) is in good agreement with the numerical result for small k . One can see from inspection of Fig. 5 and analysis of the run parameters here that this case is stabilized by two-fluid (Hall) effects. There is good agreement with the local dispersion relation,⁸ which predict stabilization at $\omega^*/\gamma_M = 2$, with the exception of those calculations including ion kinetic effects. There is a transition near the fluid stabilization point in which the mode for which the local dispersion relation applies (that with largest x scale size) is displaced by a mode with higher x structure and with a higher growth rate.

The mode transition is shown in Fig. 6 where perturbed density contours are shown for three cases near the transition point. As can be seen, the “fundamental” mode with large x scale is displaced by a higher x structure mode with higher growth rate.

Similar physics is observed in a high β case. The parameters are

$$\beta = 1.0, \quad T_e/T_i = 0, \quad X/L = 0.4, \quad L/d_i = 235.9,$$

$$g/d_i \Omega_{ci}^2 = 1.195 \times 10^{-5}; \quad \gamma_M/\Omega_{ci} = 2.252 \times 10^{-4}.$$

In order to examine only ion kinetic effects on the MHD modes, calculations were carried out with the Hall terms in the Ohm’s law neglected. The stability boundary using small orbit theory is not known exactly in this case, but other

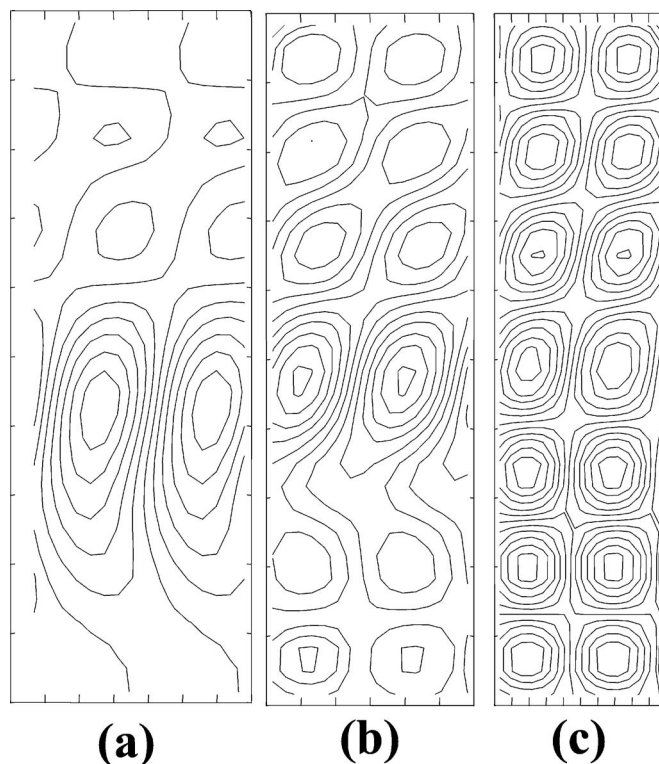


FIG. 6. Contours of perturbed density at late time for values of ω^*/γ_M near the transition point at 2.0 for the low β case. The y scale is enlarged by $5 \times$ compared with the x scale. Values are: $\omega^*/\gamma_M =$ (a) 1.76; (b) 2.06; (c) 2.47.

authors²⁸ have found a boundary of $\omega/\omega^* = 1.2 - 1.56$ for similar cases. It is not appropriate to repeat exactly those calculations as they are in a regime where $k\rho_i \gg 1$ and no connection with small orbit theory is possible.

For these calculations, the mesh used was 30×32 , $\delta t = \Delta t / 100 = 0.4618 / \Omega_{ci}$, and 25 particles per cell were loaded with the previously described high v weighted distribution. Figure 7 shows growth rates versus ω/ω^* . The MHD growth rate, driven almost entirely by the Raleigh–Taylor mechanism, is not attained at small k , because the x domain size becomes larger than the y wavelength, lowering the growth rate. Again, there seems agreement with the small orbit fluid

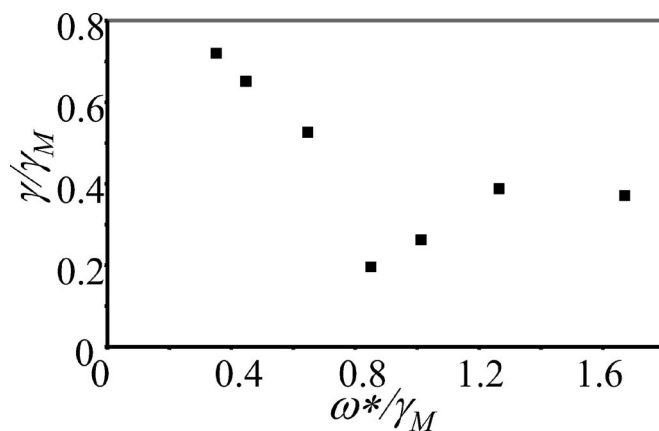


FIG. 7. Variation of growth rate with k for the high β case.

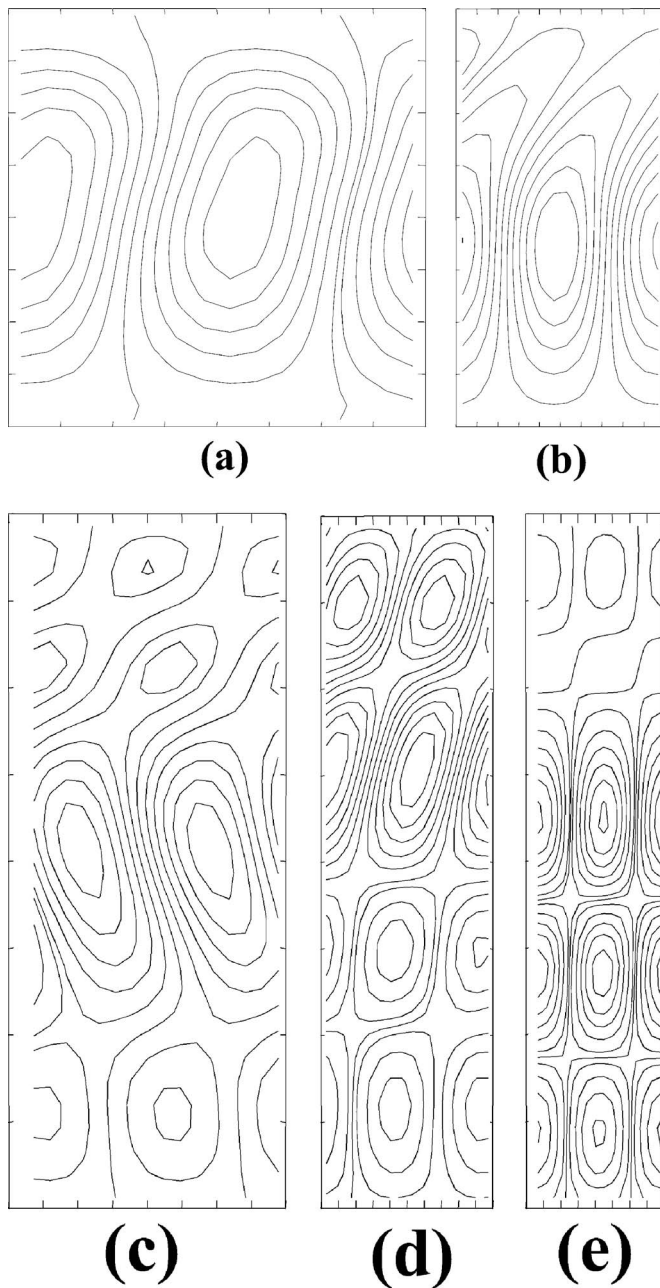


FIG. 8. Contours of perturbed density at late time for values of ω^*/γ_M near the transition point at 1.0 for the high β case. The y scale is the same as the x scale. Values are: $\omega^*/\gamma_M =$ (a) 0.35; (b) 0.65; (c) 0.85; (d) 1.27; (e) 1.67.

theory for stabilization below some threshold in ω/ω^* , while there is a transition to a higher x structure mode at larger values.

The mode structure is shown in Fig. 8, where contours of perturbed density are again illustrated. There is clearly a similar transition to the low β case in which the fundamental mode is displaced by a higher x structure mode with a higher growth rate. While there is no adequate theory which can confirm these results in detail, the behavior exhibited here has been observed in many other kinetic ion calculations. For example, in FRC stability calculations with kinetic ions,^{19–22} a similar transition from the fundamental mode to modes with higher structure is observed. Thus, kinetic ions will de-

feat the absolute stability predicted by small orbit fluid models. It is likely that resonant ion effects are responsible for the unstable modes observed in highly kinetic situations.

V. EXTENSIONS OF THE ALGORITHM

Various extensions of the closure algorithms are outlined in this section.

A. Implicit time differencing for current closure

The current closure scheme can incorporate implicit time differencing. The simplest approach would use the momentum Eq. (8) to estimate the time advanced velocity \mathbf{u} , and then the Ohm's law (4) to find the time advanced \mathbf{E} . The stress terms which occur in Eq. (10) can be estimated from δf , but the predicted fluid velocity would be replaced by the ion current as given by Eq. (6). This closely parallels the implicit moment PIC method, but in terms of δf , rather than full PIC.

B. Arbitrary polarization

The IMP2 algorithm described for TE polarization can be directly extended to arbitrary polarization. The Yee²⁵ mesh indicated in Fig. 1 is extended in the usual way to include E_z, B_x, B_y . The fluid velocity is centered with \mathbf{B} . The implicit solve requires the use of the full \mathbf{W} and \mathbf{B} operators, as described in Ref. 1.

C. Nonuniform temperature

The model described here can also be extended to the case of nonuniform background T . Since the Vlasov equation is linear, the uniform T Maxwellian used here for the equilibrium distribution can be replaced by the superposition of an arbitrary number of such distributions. The equations of motion have to be slightly modified to accommodate this superposition. In this approach, the superposition is represented by assigning a random equilibrium T to each marker particle, so that the ensemble represents the desired superposition. One can show that such an approach can represent most backgrounds of interest. The main constraint is that the density must be expressible as a function of the potential energy. This holds for MHD equilibrium with and without rotation, for example. The details of this extension will be the subject of a future paper.

VI. DISCUSSION AND CONCLUSIONS

Two new δf particle methods for closure of the extended MHD equations are developed and tested in this work. The moment equations are closed at a low-velocity moment, compared with the third or fourth order velocity moments required by CEL or QIP. In fact, either a first order velocity moment (current closure) is computed from marker particles with a fixed background δf method, or a second order moment (stress closure) is computed with a simple evolving background method. Closure with low-order velocity moments is effective in limiting the noise which is inevitable in particle methods to a level that the closure moments are useful. While there can be many possible implementations, the

authors have experienced many methods that do not work as well, even to the degree that they have not been useful in any practical calculation. Thus, the methods developed here are recommended as useful starting points for closure of the moment equations.

In the current closure scheme, the usual equation evolves δf from the electric field \mathbf{E} . Then the ion current (flow velocity) \mathbf{u} is calculated from δf , and the remaining equations are advanced. It is not necessary to advance the particle conservation (continuity) equation, in this approach, as δf also provides the perturbation number density.

In the stress closure scheme, the background distribution evolves in number density and flow velocity, and the evolution equation for δf involves only the gradient of the flow velocity \mathbf{u} . In this approach, additional moment equations for the number density and \mathbf{u} are advanced in time, and the closure is the perturbation ion stress Π_i .

Both methods seem to have comparable accuracy, as determined by several numerical tests. In one dimension, both methods reproduce the three waves for $k_{\perp}=0$ and show good agreement with one another and with the analytic dispersion relation for ion-acoustic waves, both for the real frequency and the (Landau) damping. A series of two-dimensional tests were also carried out for the opposite polarization ($k_{\parallel}=0$) and good agreement with the low-frequency G-mode was demonstrated.

One can also see that both approaches can achieve comparable accuracy for low phase velocity waves. We consider the scaling for 1D polarization ($k_{\perp}=0$). In this case, the size of δf for the current closure approach is found from Eq. (15) to be $\delta f \approx e v_{\phi} E \bar{f}(v_{\phi}) / M \bar{v}_T^2 \omega_{\text{orb}}$, where v_{ϕ} is the phase velocity and ω_{orb} a relevant orbital frequency, giving a contribution to the velocity of magnitude $u \approx e v_{\phi}^2 E \bar{f}(v_{\phi}) / P \omega_{\text{orb}}$, with P as the species pressure. On the other hand, we find from Eq. (26) that the weight is of size $\tilde{h} \approx v_{\phi}^2 k u / \bar{v}_T^2 \omega_{\text{orb}}$, giving the stress $\tilde{\Pi} \approx M v_{\phi}^4 k u \bar{f}(v_{\phi}) / \bar{v}_T^2 \omega_{\text{orb}}$, and the velocity $u \approx v_{\phi}^4 k^2 u \bar{f}(v_{\phi}) / \omega \bar{v}_T^2 \omega_{\text{orb}}$. Since $u = eE / M\omega$ these two contributions are of exactly the same size. Further, the typical δf term is of comparable size for the two formulations, with the additional velocity weight giving only a factor of 2 increase in the size of high v contributions to δf for the stress closure compared with the current closure.

Of course, high phase velocity waves are treated equally well with both methods as well, as demonstrated, for example by the ion acoustic tests presented previously. Notice that the low-noise resolution of low phase velocity waves by stress closure depends crucially on the particular method used here. The authors have experienced unacceptable behavior when the conventional δf method is used to compute the stress closure, and its use is not recommended for that reason.

Both closure schemes satisfy system conservation laws with sufficient accuracy. The current closure is simpler to implement and may be more easily extensible, although the inclusion of orbit averaging and/or implicit time differencing has not yet been considered. For incorporating these latter features, the stress closure approach has certain advantages. First, \mathbf{E} does not enter the kinetic portion of the problem, so

the moment equations can be implicitly advanced with conventional methods and a simple iteration used to make the kinetic and moment portions fully implicit.

In addition, there is an exact energy conservation law for discrete systems using the stress closure approach. Part of the conserved energy is the root mean square sum of the particle weights (actually a slightly more complicated convex function occurs in the nonlinear case). Because the remaining components of the energy are positive definite, this assures that secular growth of δf cannot occur, resolving a source of uncertainty associated with previous formulations which use a fixed background. A stability comparison shows that the discrete system is more stable than a physical comparison system whose stability properties are well understood. Several new features are essential to these properties: (1) use of a fixed temperature evolving background distribution; (2) use of the particular velocity in the particle description; (3) projection of the unknown perturbation distribution so that low-order velocity moment constraints are satisfied exactly; and (4) proper space and time centering of the discrete quantities.

Extensions of the present work to include nonlinearity, arbitrary polarization, and arbitrary background temperature variation are outlined. The methods described here are natural partners to modern extended MHD studies of low-frequency modes for which kinetic modifications are all important. It is expected that these methods may contribute greatly to these studies.

As a coda, we briefly discuss two points which have been raised by our colleagues (including the referee) with whom we have been fortunate to discuss this work. These are (1) incorporation of collisions into either of our closure schemes and (2) the relation between the bound of $\langle \delta f^2 \rangle$ and the production of entropy in the presence of (in particular) background temperature gradients.

With regard to the first point, the current closure approach can directly apply all the machinery previously developed^{29,30} for fixed background δf methods. Some work along similar lines has also been done for evolving background δf formulations³¹ and may be adapted to the stress closure algorithm given here.

An interesting alternative is suggested by the construction of the representation here to assure that the first two velocity moments of δf vanish [Eq. (25) and subsequent discussion]. That is, this would seem to vitiate the original argument given³⁰ against the application of a binary collision approach to δf which noted that there are too many conservation laws to admit a binary collision process which conserves all relevant quantities. In the present formulation, the first two (actually four quantities) conservation laws for the first order distribution are incorporated into the representation. The counting now shows that there are three free parameters, if we consider a binary collision of two δf particles which conserves the sum squared weights (with the appropriate *a priori* weighting). These may be taken to be the Euler angles for the orbits velocity vectors in the center-of-mass frame, and some interchange of the particle weights. It seems likely that it would be possible to construct a Monte Carlo realization of the collision operator which not only respects all conservation laws, but also leads to a realization

of the desired self-collision operator. This interesting question will have to await future work.

Finally, how does one reconcile a bounded $\langle \delta f^2 \rangle$ given by the stress closure approach with the increase of entropy inherent in turbulent transport in the presence of a temperature gradient? The answer appears to be that the evolving background leads to entropy generation by coarse graining. In the approach suggested in Sec. V, the background n and T are both function of a single quantity (an effective potential). This implies that there will arise a turbulent \tilde{T} in the presence of $\nabla \tilde{T}$. The coarse graining of this turbulent field leads to an effective thermal conductivity, as in any fluid, and this leads in turn to either a relaxation of $\nabla \tilde{T}$ or to a constant heat flux, depending on the boundary conditions and presence or absence of heat sources and sinks. It thus appears that turbulent heat transport can be addressed by the methods outlined here while maintaining a bounded $\langle \delta f^2 \rangle$ for all times.

ACKNOWLEDGMENTS

D.C.B. would like to thank the NIMROD team for many helpful discussions during the past four years of work on this topic. Earlier contributions by Carl Sovinec and Dave Nystrom at Los Alamos and Jim Peobles at Boulder are also acknowledged.

This work was supported by the U.S. Department of Energy, Office of Fusion Energy Sciences.

APPENDIX: ENERGY CONSERVATION FOR THE DISCRETE STRESS CLOSURE SYSTEM

A special property of the stress closure difference equations is that there exists a conserved energy for the discrete system, while previous δf implementations recover energy conservation only in the continuum limit of infinitely many particles. Furthermore, the conserved energy provides a bound on the growth of the weights in time, which resolves a long-standing problem with previous δf methods.

The derivation begins by constructing the conservation law for the sum of kinetic, magnetic, and gravitational energy density in the usual manner. Taking the dot product of Eq. (8) with \mathbf{u} and using Eq. (10), combining with the dot product of Eq. (2) with \mathbf{J} and of Eq. (1) with \mathbf{B} , and writing $\mathbf{g} = -\nabla \phi$ with $\partial \phi / \partial t = 0$ gives the conservation law

$$\frac{\partial}{\partial t} \left(\frac{Mnu^2}{2} + Mn\phi + \frac{B^2}{2\mu_0} \right) + \nabla \cdot \left(\frac{Mnu^2}{2} + Mn\phi + \frac{\mathbf{E} \times \mathbf{B}}{\mu_0} \right) \mathbf{u} = -\mathbf{u}_e \cdot \nabla P_e - M\bar{v}_T^2 \mathbf{u} \cdot \nabla n + M\mathbf{nu} \cdot \tilde{\mathbf{A}}. \quad (\text{A1})$$

It remains only to manipulate the electron and ion stress terms on the right-hand side of Eq. (A1). The electron pressure is brought into conservation form using Eq. (10), which can be rewritten as

$$\frac{\partial}{\partial t} \frac{P_e}{\Gamma_e - 1} + \nabla \cdot \frac{\Gamma_e}{\Gamma_e - 1} P_e \mathbf{u}_e = \mathbf{u}_e \cdot \nabla P_e. \quad (\text{A2})$$

The fluidlike ion pressure term [second on the right-hand side of Eq. (A1)] can be manipulated in a similar manner to yield

$$\frac{\partial}{\partial t} n \log n + \nabla \cdot n(1 + \log n) \mathbf{u} = \mathbf{u} \cdot \nabla n, \quad (\text{A3})$$

giving the final fluid form

$$\frac{\partial}{\partial t} \left(\frac{Mnu^2}{2} + Mn\phi + \frac{B^2}{2\mu_0} + \frac{P_e}{\Gamma_e - 1} + M\bar{v}_T^2 n \log n \right) + \nabla \cdot \left\{ \left[\frac{Mnu^2}{2} + Mn\phi + \frac{\mathbf{E} \times \mathbf{B}}{\mu_0} + M\bar{v}_T^2 n(1 + \log n) \right] \mathbf{u} + \frac{\Gamma_e P_e}{\Gamma_e - 1} \mathbf{u}_e \right\} = M\mathbf{nu} \cdot \tilde{\mathbf{A}}. \quad (\text{A4})$$

The derivation to this point is standard, although the details of this particular two-fluid form are not usual. A final step shows the advantage of the particular δf form described previously. The identity of Eq. (31) can be rewritten as an integral

$$\frac{d}{dt} \left\{ -M\bar{v}_T^2 \sum_i W_i [\log(1 - \tilde{h}_i) + \tilde{h}_i] \right\} = -M \int d\mathbf{x} \mathbf{nu} \cdot \tilde{\mathbf{A}}. \quad (\text{A5})$$

Combining Eqs. (A4) and (A5), the final conserved quantity is

$$\mathcal{W} \equiv \int d\mathbf{x} \left[\frac{Mnu^2}{2} + Mn\phi + \frac{B^2}{2\mu_0} + \frac{P_e}{\Gamma_e - 1} + M\bar{v}_T^2 n \log n \right] - M\bar{v}_T^2 \sum_i W_i [\log(1 - \tilde{h}_i) + \tilde{h}_i]. \quad (\text{A6})$$

Since the function $-\log(1-x)-x$ is always non-negative, the last term of Eq. (A6) is also non-negative. The remaining term is the energy of an exactly equivalent system with the kinetic ions replaced by isothermal fluid ions. In the usual manner, these two observations imply that the kinetic system, after discretization, is more stable than the isothermal fluid ion system. Hence, no spurious instabilities are associated with the discretization of the kinetic problem.

A second important conclusion from the conservation of W is that the particle weights are bounded for all time. The last term of Eq. (A6) is approximately proportional to the usual norm of these weights $\sum_i W_i \tilde{h}_i^2$, giving a bound on the growth of the weights in time. Nor is this conclusion affected by considering the weights to have finite size, as the function previously considered is convex over the entire domain.

¹C. R. Sovinec, A. H. Glasser, T. A. Gianakon, D. C. Barnes *et al.*, J. Comput. Phys. **195**, 355 (2004); H. R. Strauss and W. Park, Phys. Plasmas **5**, 2676 (1998).

²S. E. Parker, Y. Chen, W. Wan, B. I. Cohen, and W. M. Nevins, Phys. Plasmas **11**, 2594 (2004); Z. Lin, T. S. Hahn, W. W. Lee, W. M. Tang, and R. B. White, Science **281**, 1835 (1998).

³S. E. Parker and W. W. Lee, Phys. Fluids B **5**, 77 (1993).

⁴Z. Chang and J. D. Callen, Phys. Fluids A **4**, 1167 (1992); **4**, 1182 (1992).

⁵B. I. Cohen, T. A. Brengle, D. B. Conley, and R. P. Fries, J. Comput. Phys. **38**, 45 (1980); B. I. Cohen, R. P. Fries, and V. Thomas, *ibid.* **45**, 345 (1982).

⁶M. Kotschenreuther, Paper PT20 in *Proceedings of the 14th Conference on Numerical Simulation of Plasmas* (SAIC-NRL, Annapolis, MD, 1991).

⁷A. Dimits, private communication (2007). This work was also presented by Andris Dimits in a Sherwood 2007 paper "Energy conservation in

- linear and perturbative δf -PIC simulations," which may be requested by contacting dimits1@llnl.gov.
- ⁸D. D. Schnack, D. C. Barnes, D. P. Brennan, C. C. Hegna, E. Held, C. C. Kim, S. E. Kruger, A. Y. Pankin, and C. R. Sovinec, *Phys. Plasmas* **13**, 058103 (2006).
- ⁹D. C. Barnes and R. A. Nebel, Paper PWE6, in *Proceedings of the 14th Conference on Numerical Simulation of Plasmas* (SAIC-NRL, Annapolis, MD, 1991); B. I. Cohen, A. M. Dimits, J. J. Stimson, and D. C. Barnes, *Phys. Rev. E* **53**, 2708 (1996); S. Brunner, E. Valejo, and J. A. Krommes, *Phys. Plasmas* **6**, 4504 (1999).
- ¹⁰S. E. Parker and J. Peobles, private communication (2005).
- ¹¹S. T. Jones and S. E. Parker, *J. Comput. Phys.* **191**, 322 (2003).
- ¹²M. A. Shay, J. F. Drake, R. E. Denton, and D. Biskamp, *J. Geophys. Res.* **103**, 9165, DOI: 10.1029/97JA03528 (1998).
- ¹³J. Nakabayashi and S. Michida, *Geophys. Res. Lett.* **24**, 1339, DOI: 10.1029/97GL01206 (1997).
- ¹⁴D. Krauss-Varban and N. Omida, *Geophys. Res. Lett.* **21**, 73, DOI: 10.1029/93GL03382 (1994).
- ¹⁵D. Biskamp, *Phys. Fluids* **29**, 1520 (1986).
- ¹⁶D. Biskamp, E. Schwarz, and J. F. Drake, *Phys. Plasmas* **4**, 1002 (1997).
- ¹⁷V. M. Vasyliunas, *Rev. Geophys.* **13** 303, DOI: 10.1029/RG013i001p00303 (1975).
- ¹⁸M. E. Mandt, R. E. Denton, and J. F. Drake, *Geophys. Res. Lett.* **21** 73, DOI: 10.1029/93GL03382 (1994).
- ¹⁹E. V. Belova, S. C. Jardin, H. Ji, M. Yamada, and R. Kulsrud, *Phys. Plasmas* **7**, 4996 (2000).
- ²⁰R. D. Milroy, D. C. Barnes, R. C. Bishop, and R. B. Webster, *Phys. Fluids B* **1**, 1225 (1989).
- ²¹A. Ishida, H. Momota, and I. C. Steinhauer, *Phys. Fluids* **31**, 3024 (1988).
- ²²D. C. Barnes, J. L. Shwarzmeier, H. R. Lewis, and C. E. Seyler, *Phys. Fluids* **29**, 2616 (1986).
- ²³G. Hu and J. A. Krommes, *Phys. Plasmas* **1**, 863 (1994).
- ²⁴C. K. Birdsall and A. B. Langdon, *Plasma Physics via Computer Simulation* (Institute of Physics, Philadelphia, 1991), p. 59.
- ²⁵K. S. Yee, *IEEE Trans. Antennas Propag.* **14**, 302 (1966).
- ²⁶M. N. Rosenbluth, N. A. Krall, and N. Rostoker, *Nucl. Fusion Suppl.* **1**, 143 (1962); K. V. Roberts and J. B. Taylor, *Phys. Rev. Lett.* **8**, 197 (1962).
- ²⁷E. N. Parker, *Astrophys. J.* **145**, 811 (1966).
- ²⁸N. M. Ferraro and S. C. Jardin, *Phys. Plasmas* **13**, 092101 (2006).
- ²⁹X. Xu and M. N. Rosenbluth, *Phys. Fluids B* **3**, 627 (1991); M. Sasinowski and A. Boozer, *Phys. Plasmas* **2**, 613 (1995); Z. Lin, W. Tang, and W. Lee, *Phys. Rev. Lett.* **78**, 456 (1997).
- ³⁰A. M. Dimits and B. I. Cohen, *Phys. Rev. E* **49**, 709 (1994).
- ³¹S. Brunner, E. Valeo, and J. A. Krommes, *Phys. Plasmas* **6**, 4504 (1999).